Towards a Unified Description of the Rheology of Hard-Particle Suspensions

B. M. Guy, M. Hermes, and W. C. K. Poon
SUPA, School of Physics and Astronomy, The University of Edinburgh, King's Buildings, Peter Guthrie Tait Road, Edinburgh EH9 3FD, United Kingdom

(Received 17 March 2015; revised manuscript received 14 June 2015; published 20 August 2015)

The rheology of suspensions of Brownian, or colloidal, particles (diameter $d \lesssim 1$ μm) differs markedly from that of larger grains ($d \gtrsim 50$ μm). Each of these two regimes has been separately studied, but the flow of suspensions with intermediate particle sizes (1 μm $\lesssim d \lesssim 50$ μm), which occur ubiquitously in applications, remains poorly understood. By measuring the rheology of suspensions of hard spheres with a wide range of sizes, we show experimentally that shear thickening drives the transition from colloidal to granular flow across the intermediate size regime. This insight makes possible a unified description of the (noninertial) rheology of hard spheres over the full size spectrum. Moreover, we are able to test a new theory of friction-induced shear thickening, showing that our data can be well fitted using expressions derived from it.

DOI: 10.1103/PhysRevLett.115.088304 PACS numbers: 83.60.Rs, 45.70.-n, 47.57.J-, 83.80.Hj

Complex fluids, polymers, colloids, and surfactant solutions find wide applications, partly because of their highly tunable behavior under deformation and in flow. The success of the mean-field "tube" model for polymers [1], which describes how each chain is constrained by thousands of neighbors, means it has long been possible to predict *ab initio* their linear and nonlinear rheology from the molecular topology with very few free parameters. In particular, a scaling description is available of the dependence of rheology on molecular weight.

However, progress in suspension rheology has been more difficult [2]. The small number of nearest neighbors (order 10) rules out any mean-field description: local details matter. It is now possible to predict the low-shear viscosity of a suspension of Brownian hard spheres (HS, diameter $d \lesssim 1$ μm) up to volume fractions of $\phi \lesssim 0.6$, and the rheology of granular HS ($d \gtrsim 50$ μm) is increasingly being studied. Surprisingly, however, how the rheology of HS changes over the whole size spectrum remains unknown, because the behavior in the industrially ubiquitous intermediate size regime, $1 \lesssim d \lesssim 50$ μm, has not been systematically explored. We offer such an exploration in this Letter, and show that the physics bridging the colloidal and the granular regimes is shear thickening.

The rheology of colloidal HS is well known [3–5]: the viscosity is determined by the particle volume fraction ϕ and the dimensionless shear rate, or Péclet number, Pe ($= \tau_B\dot{\gamma}$, the shear rate $\dot{\gamma}$ nondimensionalized by the Brownian time τ_B needed for a free particle to diffuse its own radius). At $\mathrm{Pe} \ll 1$ the flow is Newtonian; the viscosity becomes immeasurably large at $\phi_g \approx 0.58$ [5,6]. Shear thinning starts at $\mathrm{Pe} \lesssim 1$, reaching a second Newtonian regime at $\mathrm{Pe} \gg 1$ with a viscosity that diverges at random close packing [2], $\phi_{\mathrm{RCP}} \approx 0.64$, the densest amorphous packing for lubricated (frictionless) HS.

Since τ_B scales as d^3, granular HS inhabit the $\mathrm{Pe} \gg 1$ regime at all practical shear rates. Extrapolating naively from the above description of colloidal flow, one expects Newtonian behavior with a viscosity diverging at ϕ_{RCP}. Experiments do find a Newtonian viscosity, but it diverges at a ϕ that is lower than ϕ_{RCP} [7], the precise value being dependent on interparticle friction [8].

How suspension rheology transitions from colloidal to granular behavior as d increases has not been theoretically predicted, and remains experimentally unclear. Previous experiments on size dependence [3,4,9] stayed in the colloidal regime, or used highly polydisperse systems near the granular limit [10]. Thus, no unified description over all particle sizes is yet available.

We study the rheology of the intermediate size regime using poly-methylmethacrylate (PMMA) spheres sterically stabilized by poly-12-hydroxystearic acid (PHSA) with $d = 268$ nm to 45 μm, dispersed in a density-matching solvent, Fig. 1. We show that the transition from colloidal to granular behavior is driven by the widespread phenomenon of shear thickening [11] at a critical "onset stress," whose scaling with particle size ($\propto d^{-2}$), Fig. 2, differs from that of the intrinsic stress scale ($\propto d^{-3}$). Understanding this complexity leads to a unified description of hard-particle rheology over the whole range of d, Fig. 3. Interestingly, our results also confirm recent theory and simulations [8,12,13] ascribing shear thickening to the formation of frictional contacts.

We used PMMA particles stabilized by 5–10 nm PHSA "hairs" [25] in a density-matching mixture of cycloheptylbromide or cyclohexylbromide and decalin. We present data for $d = 404$ nm (from static light scattering), 3770 nm (from microscopy) particles with polydispersity ~10% (from light scattering and electron microscopy, respectively). Data for $d \approx 280$ nm (in decalin), 268, 912, 1800,

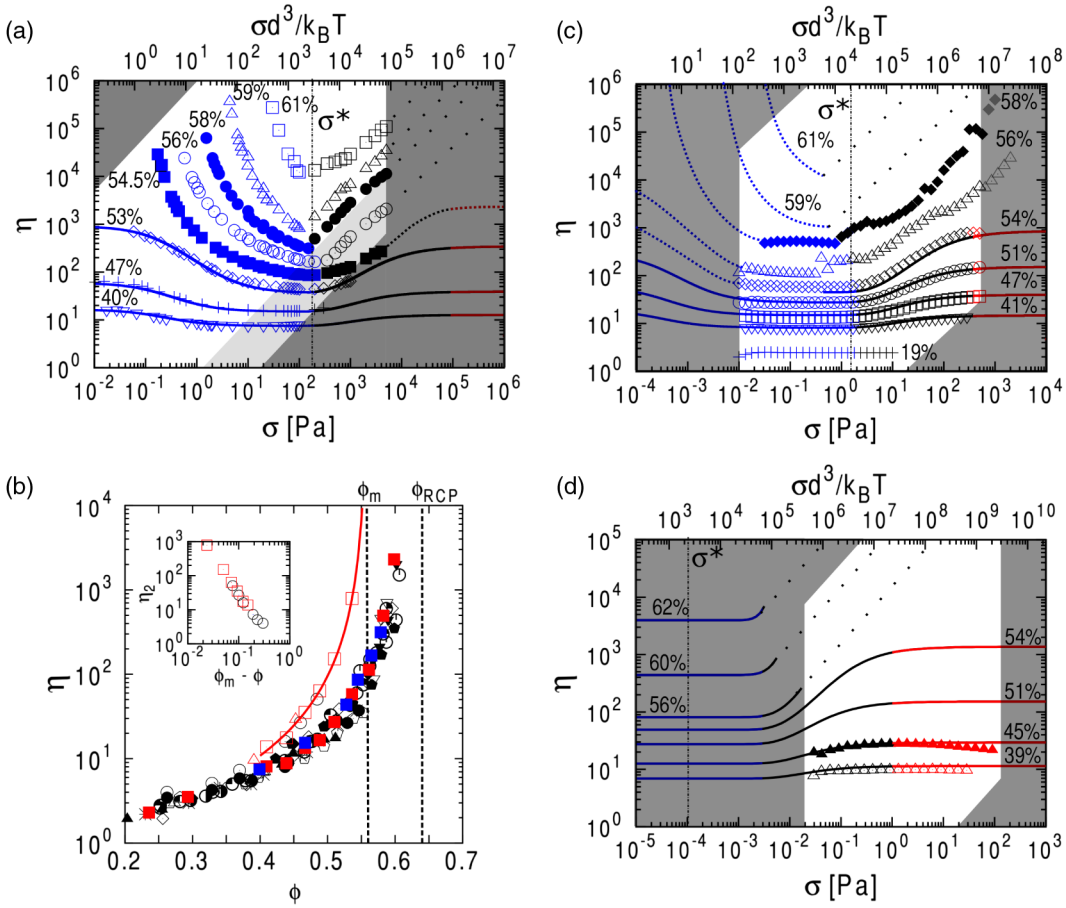

FIG. 1 (color online). Rheology in the colloidal, intermediate, and granular size regimes. (a) Relative viscosity η versus shear stress σ in units of Pa and k_BT/d^3 for $d = 404$ nm spheres at different volume fractions (%), as labeled. Solid lines, fits based on [12]; finely dotted lines, schematics based on literature data (with sparsely dotted = unstable states). Samples shear thicken above a ϕ-independent onset stress σ^* (vertical dashed line). Color scheme: blue, frictionless interactions ($\sigma < \sigma^*$); black, shear thickening; red, frictional interactions ($\sigma \gg \sigma^*$). The unshaded region is accessible using our rheometer, which reaches maximum and minimum shear rates of 8000 and 10^{-3} s^{-1}, respectively, and a minimum stress of 10^{-2} Pa; the maximum accessible stress is set by a d-dependent fracture stress $\sigma^\dagger$. (b) Main: $\eta(\phi)$ for the limiting high-shear viscosity, η_1, in (a) [blue (dark gray) filled square]; the lower, $\eta_1(\phi)$ [red (light gray) filled square], and upper, $\eta_2(\phi)$ (red square), branches in (c); the upper branch (red triangle) in (d). Solid red line, least squares fit to $\eta_2(\phi) = A(1 - \phi/\phi_m)^{-n}$ with $A = 0.20(9)$, $\phi_m = 0.558(5)$ and $n = 2.2(2)$. $\eta_1(\phi)$ data for other sizes of PMMA spheres in this work, $d = 912$ nm (triangle down) and 1800 nm (filled triangle down). Other symbols, literature high shear viscosities (with ϕ shifted by up to 5%) for sterically stabilized PMMA [5,6,14,15], sterically stabilized silica [3], and glass beads [11]. (filled circle) and (circle), lower and upper branches from [15]. Inset, $\eta_2(\phi)$ versus $(\phi_m - \phi)$ including the upper branch from [15]. (c) $\eta(\sigma)$ for $d = 3770$ nm spheres. The flow in both (a) and (c) was unsteady for $\phi \geq 0.56$, and points represent temporal averages. (d) $\eta(\sigma)$ for $d = 45$ μm spheres, with ϕ shifted up so that the data agree with $\eta_2(\phi)$ in (b).

and 4500 nm (in cycloheptylbromide and decalin) give the same picture. Samples were prepared by diluting a close packed sediment, using simulations [26] to estimate ϕ_{RCP} of polydisperse HS. The solvent viscosities were $\eta_f = 2.83$ mPa s for the large and 2.4 mPa s for the small particles at 19 °C. We also present data for 45 μm particles, prepared by mixing dry powder and solvent ($\eta_f = 2.4$ mPa s, see Supplemental Material [20]). Adding an excess of screening salt tetrabutylammonium chloride did not change the rheology; we present salt-free data.

Rheology was performed in an Anton Paar 301 rheometer in truncated cone and plate geometry (cone angle 1°, radius 25 mm, truncation gap 100 μm) in stress-controlled mode unless otherwise stated. A sandblasted cone (surface roughness $\sim$10 μm) and a base plate roughened with silicon carbide powder (surface roughness $\sim$5 μm) were used. Rheology of the 45 μm particles was performed in a parallel plate geometry (see Supplemental Material [20]). Even with a solvent trap, artifacts due to drying were evident if samples were left to equilibrate at shear rates $\dot{\gamma} \lesssim 10^{-2}$ s^{-1}. Thus, we worked at $\dot{\gamma} > 0.01$ s^{-1}.

To establish a baseline, we first explore $d = 404$ nm colloids. Figure 1(a) shows the relative viscosity $\eta = (\sigma/\dot{\gamma})/\eta_f$ (solvent viscosity $\eta_f = 2.4$ mPa s) as a function

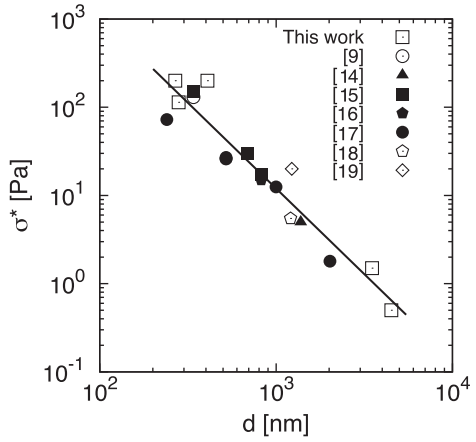

FIG. 2. Onset stress σ^* versus particle diameter d for PHSA-stabilized PMMA spheres in this and previous [9,14,16–19] work. The solid line is a least-squares fit to a power law $\sigma^* = Bd^\alpha$, with $B = 7 \times 10^{-11}$ J nm$^{-1.1}$ and $\alpha = -1.9(1)$.

of applied shear stress σ. The region in each $\eta(\sigma)$ plot in Fig. 1 *not* shaded dark gray is the "observable window" accessible by conventional rheology, and points are experimental data. Additionally, the light gray region in Fig. 1(a) is accessible but typically not probed in previous work [3,5].

Our data for $\phi = 0.40$ and 0.47 show classic shear thinning to a high-shear Newtonian plateau $\eta_1(\phi)$ in the observable window. The $\phi = 0.53$ sample behaves similarly in this window, but shear thickens beyond it. At $\phi = 0.56$, we see the onset of discontinuous shear thickening, i.e., the gradient $d\log\eta/\log\sigma$ reaches 1, corresponding to a vertical flow curve, $d\dot{\gamma}/d\sigma = 0$. Our $\eta_1(\phi)$ data, Fig. 1(b) [blue (dark gray) filled square], agree with previous measurements of the "high-shear viscosity" of various colloids [3,5,6,14,15]. Within experimental uncertainty, shear thickening begins at a fixed "onset stress," $\sigma^* \simeq 200$ Pa, for all ϕ. At a higher ϕ-independent stress $\sigma^\dagger \simeq 10^5$ Pa, samples fracture—this is the high-σ boundary to the observable window. (The lower right, slanted, boundary is due to an inertial instability expelling samples from the instrument.)

Increasing d by an order of magnitude to 3770 nm has a dramatic effect on the rheology in the observable window, Fig. 1(c). Now, at $0.41 \le \phi \le 0.54$, there is a transition from a lower to a higher, shear-thickened, Newtonian plateau as σ increases [11,27]. The transition to a shear-thickened state again begins at a ϕ-independent onset stress, now at $\sigma^* \simeq 2$ Pa. Approximately the same onset stress applies at $\phi \ge 0.56$, but now the high-shear plateau vanishes. The data become noisy and $d\log\eta/d\log\sigma \simeq 1$, which is the discontinuous shear thickening limit. The onset of fracturing in the sample is now at $\sigma^\dagger \simeq 500$ Pa, above which the data show poor reproducibility and strong history dependence.

The two plateau viscosities for the $d = 3770$ nm particles fall on separate diverging branches, Fig. 1(b) [red (light gray) filled square and red square]. The lower plateau viscosity here corresponds to $\eta_1(\phi)$ for the $d = 404$ nm colloids [blue (dark gray) square]: both diverge at $\phi \simeq 0.64 = \phi_{\rm RCP}$. Thus, we infer an experimentally inaccessible shear thinning regime for these particles at lower σ, sketched schematically in Fig. 1(c). The high viscosity branch $\eta_2(\phi)$ diverges at $\phi_m \simeq 0.55 < \phi_{\rm RCP}$. Interestingly, this is close to random loose packing for frictional granular spheres [28]. We infer a corresponding regime of shear thickening to a plateau viscosity in the 404 nm particles outside the observable window, Fig. 1(a). Two viscosity branches can be extracted from previous work on PMMA spheres [15]; each extracted branch can be collapsed onto our corresponding branch by a small shift in ϕ [Fig. 1(b)]. Note that it would be meaningless (though mathematically possible) to collapse the two branches in Fig. 1(b) into a single curve by a large ($\sim$0.1) shift in ϕ: these branches are observed together in the same experiment, and correspond to distinct phenomena.

Recent theory [12] and simulations [8,13] predict just such a two-branch structure for the viscosity in non-Brownian suspensions, and shear thickening is associated with a transition from the low- to the high-viscosity branch above an onset stress σ^* (see also [29]). At $\sigma \ll \sigma^*$, particles do not touch and all contacts in the system are lubricated, while for $\sigma \gg \sigma^*$, all particles are pressed into frictional contact. The point at which the high-viscosity branch diverges, ϕ_m, decreases with increasing (static) friction coefficient μ_p between particles [8], and $\phi_m = \phi_{\rm RCP}$ only if $\mu_p = 0$. Our data for particles in the transitional size regime, Fig. 1(c), are consistent with this scenario; indeed, the solid lines are fits of our data to theory [12] (see Supplemental Material [20] for details).

The onset stress in this theory σ^* arises physically from the presence of barriers, e.g., from PHSA hairs in our case, that stabilize particles against entering the primary van der Waals minimum of their mutual interaction potential, and therefore prevent interparticle contact. When the applied stress exceeds a critical value σ^*, however, these barriers are overcome and particles are pressed together to make frictional contacts.

We find, Fig. 2, that σ^* decreases with particle size as $\sigma^* \simeq Bd^\alpha$ with $B = 7 \times 10^{-21}$ J nm$^{-1.1}$ and $\alpha = -1.9$. For charged-stabilized colloids, one expects $\sigma^* \propto d^{-2}$ [2]; but charge is irrelevant in our case, because σ^* is unchanged by adding salt (data not shown). More relevantly, $\sigma^* \propto d^{-2}$ [30] and $\propto d^{-1.75}$ [16] scalings are predicted theoretically for stabilizing polymer brushes, and d^{-2} scaling is found in other sterically stabilized PMMA particles [16].

If we take our data as supporting $\sigma^* \propto d^{-2}$, then a constant force f^* is needed to push particles into frictional

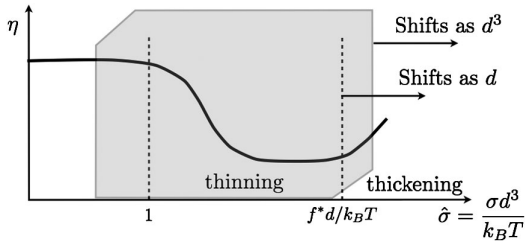

FIG. 3. Relative viscosity η versus dimensionless stress $\hat{\sigma}$. The observable window (shaded) for colloids shows shear thinning, which begins at $\hat{\sigma} \simeq 1$; shear thickening, beginning at a dimensionless onset stress of $\hat{\sigma}^* = \sigma^* d^3/k_BT = f^* d/k_BT$, occurs towards the high end of accessible stresses. As the particle diameter d increases, $\hat{\sigma}^*$ shifts right as d, and the second Newtonian regime in the $\eta(\hat{\sigma})$ curve is stretched out. However, the (shaded) observable window shifts right faster, as d^3. Thus, shear thinning becomes unobservable for intermediate particle sizes, and the shear-thickened state fills the observable window of the largest particles (grains). Figures 1(a), 1(c), and 1(d) show three snapshots of this scenario (also, see Supplemental Material Fig. S1 [20]).

contact: $\sigma^* \simeq f^*/d^2$ with $f^* = 2.4 k_B T/\text{nm}$. This is comparable to the $6 k_B T/\text{nm}$ measured between similar PHSA hairs in a different geometry [31]. The microscopic origins of this constant force $f^* \propto d^0$ are at present unclear (see [16] and Supplemental Material [20]), although $\sigma^* \propto d^{-2}$ may be generic: a d^{-2} scaling of a critical onset *shear rate* is reported in a review of diverse systems [32] (where the substantial data scatter may come from using $\dot{\gamma}$ rather than σ as the scaling variable).

The interplay between the d^{-2} scaling of the onset stress for shear thickening σ^* and the d^{-3} scaling of the intrinsic stress scale controls the colloidal to granular crossover in our system. The progression of observable rheology is set out schematically in Fig. 3 and its caption. (An alternative summary of our findings in the form of a "rheological state diagram" is shown in Supplemental Material Fig. S2 [20].) On the cusp of the granular regime, $d = 45$ μm, Fig. 1(d), the rheology in the observable window is dominated by the frictional state, with only a small amount of shear thickening visible at the far left of the window, which is, nevertheless, consistent with the theory in [12] (solid lines). The scenario outlined in Fig. 3 should be valid for any system in which $\sigma^* \propto d^{-\lambda}$ with $\lambda > 0$, with the exact value of λ controlling the sharpness of the crossover. Except for $\lambda = 3$, the different scaling of σ^* and the intrinsic stress (always $\propto d^{-3}$ for dimensional reasons) means that a single set of master curves cannot be found to describe the suspension rheology for all d.

The existence of an "onset stress" σ^* means that residual van der Waals attraction sets a practical limit to the largest particles we could in principle study. For $d \gtrsim 20$ μm, the yield stress due to van der Waals attraction exceeds σ^* above a critical volume fraction, ϕ_{gel}, so that the moment the system has yielded it flows on the frictional branch [33] (see Supplemental Material [20] for details). For the 45 μm spheres, $\phi_{\text{gel}} \approx 0.45$, so we report results for lower ϕ only, Fig. 1(d). For larger d, a proper exploration of the repulsive granular regime is not possible.

Our data also impact on the understanding of the ubiquitous phenomenon of shear thickening. One theory, e.g., [34], ascribes shear thickening to hydrodynamic interactions (HIs) alone, with interparticle friction playing no role. Simulating a system of frictionless spheres with only HIs gives a viscosity increase that is weak and continuous [35]. It is unclear how the discontinuous shear thickening we observe could arise in this framework, whereas a recent theory of friction-driven shear thickening [12] can quantitatively describe our results. We also note that the shear thickening we observe is distinct from recent work on inertial systems [36,37], as our particle Reynolds number is at most $\approx 10^{-1}$, and typically $\lesssim 10^{-4}$ at the onset of thickening.

To conclude, we have shown that the transition from colloidal to granular rheology is driven by shear thickening. Our data are consistent with recent suggestions [8,12,13] that shear thickening is associated with the development of frictional particle contacts at an onset stress σ^*, which we find to decrease with particle size as d^{-2}. Thus, particles with $d \lesssim 1$ μm will behave as frictionless, Brownian hard spheres at most accessible stresses. For intermediate-sized particles, frictionless and frictional states are observed at low and high stress, respectively. Finally, a particulate suspension is granular when σ^* is much smaller than commonly encountered stresses [38]; such a suspension is "always shear thickened." The size at which this happens depends on the "stabilising force" f^*, and therefore the surface chemistry.

That the onset stress is readily accessible and routinely exceedable for a suspension of particles with 1 μm $\lesssim d \lesssim 50$ μm, Figs. 1(c) and 2, has significant practical consequences, especially for concentrations in the range $\phi_m < \phi < \phi_{\text{RCP}}$. Once σ^* is exceeded, there is no frictional branch with finite viscosity to which the suspension may jump, Fig. 1(b). The system shear jams, and shows a qualitative change in its rheology consistent with previous work on concentrated suspensions [39]. The flow is unsteady, shows edge fracture and wall slip (confirmed by imaging), and becomes strongly history dependent.

Understanding polydisperse industrial suspensions whose particle size distributions span all three regimes remains a formidable challenge. Our unified description of particulate rheology over all sizes, summarized in Fig. 3, has laid the foundation for this challenge to be met. The data in this article are available online at http://dx.doi.org/10.7488/ds/286.

This work was funded by the U.K. EPSRC (EP/J007404/1) and a CASE studentship with Johnson Matthey. We thank Mike Cates, Paul McGuire, Chris Ness, Guilhem Poy, and Jin Sun for fruitful discussions, and Andy Schofield for particles.

[1] R. H. Colby and M. Rubinstein, *Polymer Physics* (Oxford University Press, Oxford, 2003).
[2] J. Mewis and N. J. Wagner, *Colloidal Suspension Rheology* (Cambridge University Press, Cambridge, 2012).
[3] J. C. van der Werff and C. G. de Kruif, J. Rheol. **33**, 421 (1989).
[4] I. M. Krieger, Adv. Colloid Interface Sci. **3**, 111 (1972).
[5] G. Petekidis, D. Vlassopoulos, and P. N. Pusey, J. Phys. Condens. Matter **16**, S3955 (2004).
[6] S. E. Phan, W. B. Russel, Z. Cheng, J. Zhu, P. M. Chaikin, J. H. Dunsmuir, and R. H. Ottewill, Phys. Rev. E **54**, 6633 (1996).
[7] F. Boyer, E. Guazzelli, and O. Pouliquen, Phys. Rev. Lett. **107**, 188301 (2011).
[8] R. Mari, R. Seto, J. F. Morris, and M. M. Denn, J. Rheol. **58**, 1693 (2014).
[9] J. Mewis and J. Vermant, Progress in organic coatings **40**, 111 (2000).
[10] S. C. Tsai and K. Zammouri, J. Rheol. **32**, 737 (1988).
[11] E. Brown and H. M. Jaeger, Rep. Prog. Phys. **77**, 046602 (2014).
[12] M. Wyart and M. E. Cates, Phys. Rev. Lett. **112**, 098302 (2014).
[13] R. Seto, R. Mari, J. F. Morris, and M. M. Denn, Phys. Rev. Lett. **111**, 218301 (2013).
[14] W. J. Frith, J. Rheol. **40**, 531 (1996).
[15] P. D'Haene, J. Mewis, and G. G. Fuller, J. Colloid Interface Sci. **156**, 350 (1993).
[16] L.-N. Krishnamurthy, N. J. Wagner, and J. Mewis, J. Rheol. **49**, 1347 (2005).
[17] T. A. Strivens, J. Colloid Interface Sci. **57**, 476 (1976).
[18] M. I. Smith, R. Besseling, M. E. Cates, and V. Bertola, Nat. Commun. **1**, 114 (2010).
[19] L. Isa, Ph.D. thesis, University of Edinburgh, 2007.
[20] See Supplemental Material at http://link.aps.org/supplemental/10.1103/PhysRevLett.115.088304, which includes Refs. [21–24], for details of the model used to the fit the data in Fig. 1, further discussion of the onset stress σ^*, and an alternative schematic to Fig. 3.
[21] V. Kobelev and K. S. Schweizer, Phys. Rev. E **71**, 021401 (2005).
[22] D. Howell, R. P. Behringer, and C. Veje, Phys. Rev. Lett. **82**, 5241 (1999).
[23] C. S. O'Hern, S. A. Langer, A. J. Liu, and S. R. Nagel, Phys. Rev. Lett. **86**, 111 (2001).
[24] J. N. Israelachvili, *Intermolecular and Surface Forces* (Academic Press, 2011).
[25] S. Barsted, L. Nowakowska, I. Wagstaff, and D. Walbridge, Trans. Faraday Soc. **67**, 3598 (1971).
[26] R. S. Farr and R. D. Groot, J. Chem. Phys. **131**, 244104 (2009).
[27] C. D. Cwalina and N. J. Wagner, J. Rheol. **58**, 949 (2014).
[28] L. E. Silbert, Soft Matter **6**, 2918 (2010).
[29] I. A. Bashkirtseva, A. Y. Zubarev, L. Y. Iskakova, and L. B. Ryashko, Colloid J. **71**, 446 (2009).
[30] J. Kaldasch and B. Senge, Colloid Polymer Sci. **287**, 1481 (2009).
[31] G. Bryant, S. R. Williams, Q. LinMao, I. K. Snook, E. Perez, and F. Pincet, Phys. Rev. E **66**, 060501 (2002).
[32] H. A. Barnes, J. Rheol. **33**, 329 (1989).
[33] E. Brown, N. A. Forman, C. S. Orellana, H. Zhang, B. W. Maynor, D. E. Betts, J. M. DeSimone, and H. M. Jaeger, Nat. Mater. **9**, 220 (2010).
[34] N. J. Wagner and J. F. Brady, Phys. Today **62**, 27 (2009).
[35] J. F. Brady and J. F. Morris, J. Fluid Mech. **348**, 103 (1997).
[36] N. Fernandez, R. Mani, D. Rinaldi, D. Kadau, M. Mosquet, H. Lombois-Burger, J. Cayer-Barrioz, H. J. Herrmann, N. D. Spencer, and L. Isa, Phys. Rev. Lett. **111**, 108301 (2013).
[37] T. Kawasaki, A. Ikeda, and L. Berthier, Europhys. Lett. **107**, 28009 (2014).
[38] Note that the range of accessible stresses is both rheometer specific and geometry specific (e.g., using a Couette geometry would extend the observable window in Fig. 1 by delaying the onset of edge fracture).
[39] D. Lootens, H. Van Damme, and P. Hébraud, Phys. Rev. Lett. **90**, 178301 (2003).